The Development of a MEMS Gyroscope for Absolute Angle Measurement

Damrongrit Piyabongkarn, Rajesh Rajamani, and Michael Greminger

***Abstract*—Microelectromechanical systems (MEMS) gyroscopes are typically designed to measure angular rate of rotation. A measurement of the angle itself is useful in many applications but cannot be obtained by integrating the angular rate due to the presence of bias errors which cause a drift. This paper presents an innovative design for a vibrating gyroscope that can directly measure both angle and angular rate. The design is based on the principle of measuring the angle of free vibration of a suspended mass with respect to the casing of the gyroscope. Several critical challenges have to be handled before the theoretical sensing concept can be converted into a reliable practical sensor. These include compensating for the presence of dissipative forces, mismatched springs, cross-axis stiffness and transmission of rotary torque. These challenges are addressed by the development of a composite nonlinear feedback control system that compensates for each of the above effects and ensures that the mass continues to behave as a freely vibrating structure. Theoretical analysis and simulation results presented in the paper show that the gyroscope can accurately measure both angle and angular rate for low-bandwidth applications.**

***Index Terms*—Angle measurement, angular rate, gyroscope, microelectromechanical systems (MEMS).**

I. Introduction

GYROSCOPES have played an important role in aviation, space exploration and military applications [7]. Until recently, high cost and large size made their use in automobiles and other consumer products prohibitive. With the advent of microelectromechanical systems (MEMS), gyroscopes and other inertial measurement devices can now be produced cheaply and in very small packages in the microdomain. An example of this are the MEMS accelerometers now used in some automobiles to detect collisions for air bag deployment [3].

Vibratory gyroscopes are the most common of the existing MEMS gyroscopes. Vibrating gyroscopes have a vibrating member that reacts to coriolis acceleration when the gyroscope undergoes an angular rate of rotation Ω. By measuring this reaction to the coriolis acceleration, the gyroscope's rate of rotation can be accurately measured.

In order to estimate the absolute angle θ with a traditional MEMS rate-gyroscope, one would have to integrate the angular rate signal Ω with respect to time. The problem with this method is that bias errors in the angular rate signal from the gyroscope will inevitably cause the integrated angle value to drift over time, since all gyroscopes have at least a small amount of bias error in their angular rate signal. This paper develops a sensor design to directly measure absolute angle. The design can also be combined with traditional angular rate measurement to provide a sensor in an integrated package that measures both angle and angular rate.

There are a large number of applications where a gyroscope that can measure angle would be useful. A common application is measurement of the heading or orientation of a highway vehicle. The measurement of orientation is useful in computer-controlled steering of the vehicle as well as in differential braking systems being developed by automotive manufacturers for vehicle skid control [11], [13].

An important additional benefit of the proposed technology is that it would also contribute toward improving the accuracy of the regular rate gyroscopes (see Section V). The proposed design is novel in that it breaks new ground by introducing sophisticated control systems into the MEMS domain. It is the use of advanced control techniques that leads to a new sensor making the measurement of a new variable (absolute angle) possible.

A number of researchers and research groups have worked on MEMS vibratory-rate gyroscopes. A good description of the working of a basic angular rate gyroscope can be found in [2]. Here the gyroscope consisted of a single mass oscillating longitudinally with rotation induced lateral deflections being sensed capacitively. A summary of the basic working principle of an angular rate gyroscope is also provided below in Section II.

The bulk of literature on MEMS vibratory gyroscopes deals with different embodiments of the above basic sensing concept described in [2]. There are varying designs and implementation using a number of different fabrication processes. Bernstein [1] demonstrated a tuning fork gyroscope using two masses that oscillate laterally. An external oscillation induced oscillation out of plane of the device. Juneau [5] demonstrated a dual-axis gyroscope which could simultaneously measure two rotational rates. It consisted of a rotating disk in which deflection induced by rotations about two axes were measured out of plane of the device. A gyroscope based on a vibrating ring was demonstrated by Putty [10]. The work by Kranz [6] focused on a new one-mass-inside-another design that reduced measurement errors due to mechanical crosstalk.

All of the above results relate to gyroscopes that measure angular rate. Very few papers are available in literature on gyroscopes that directly measure absolute angle [9], [17]. The use of a vibratory gyroscope for measurement of absolute angle was suggested by Friedland and Hutton in 1978.

Manuscript received September 16, 2002. Manuscript received in final form June 7, 2004. Recommended by Associate Editor F. Zhao. This work was supported by the National Science Foundation under NSF Grant CMS-0116433.

The authors are with the Department of Mechanical Engineering, University of Minnesota, Minneapolis, MN 55455 USA (e-mail: rajamani@me.umn.edu).

Digital Object Identifier 10.1109/TCST.2004.839568

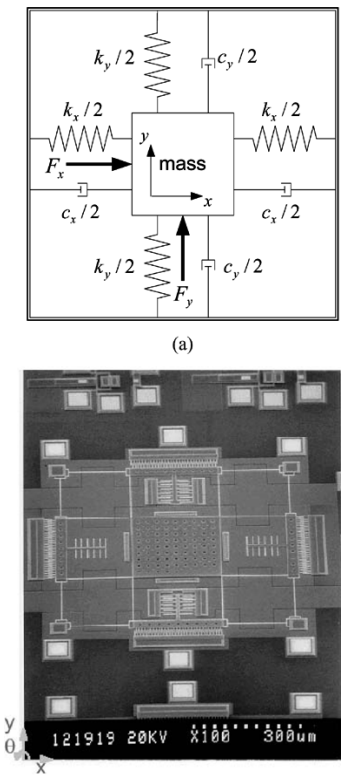

Fig. 1. Suspended mass vibrating gyroscope. (a) Schematic diagram of a vibratory gyroscope. (b) Vibratory-rate gyroscope fabricated in the MCNC MUMPs process [14].

II. Background on the Working of Angular-Rate MEMS Gyroscopes

The traditional suspended mass vibrating gyroscope consists of a mass $m$suspended by elastic members that allow it to travel in both the x and y directions as shown in Fig. 1(a). The MEMS embodiment of such a suspended mass gyroscope is shown in Fig. 1(b). The equations of motion for such a system can be represented by

$$\ddot{x} = -\omega_x^2 x - \frac{c_x}{m}\dot{x} + x\dot{\theta}^2 + y\ddot{\theta} + 2\dot{\theta}\dot{y} + \frac{F_x}{m} \tag{1}$$

$$\ddot{y} = -\omega_y^2 y - \frac{c_y}{m}\dot{y} + y\dot{\theta}^2 - x\ddot{\theta} - 2\dot{\theta}\dot{x} + \frac{F_y}{m} \tag{2}$$

where $\omega_x^2 = k_x/m, \omega_y^2 = k_y/m, c_x = 2m\xi_x\omega_x, c_y = 2m\xi_y\omega_y$, and θ is the rotation of the gyroscope casing around the z axis and F_x and F_y are controlled forces applied to the mass in the x and y directions, respectively. In order to measure the angular rate with this gyroscope, the x mode is driven sinusoidally using F_x at an amplitude of F_d and a frequency of ω_d. The frequency ω_d is usually significantly higher than the specified bandwidth of the gyroscope.

When the gyroscope experiences an external angular velocity, $\dot{\theta} = \Omega$, the $2\Omega\dot{x}$ term in (2) causes the y mode to vibrate at the driven frequency ω_d with an amplitude that is proportional to the angular rate Ω. By demodulating the y output signal at the driven frequency, the value of the angular rate can be obtained.

Note that y axis motion can also be caused by several other sources, including external forces and initial conditions. By measuring the y axis motion at only the driven frequency ω_d, we isolate the effect of the angular rotation Ω on y axis motion. Thus, angular rate can be measured accurately in spite of other external disturbances.

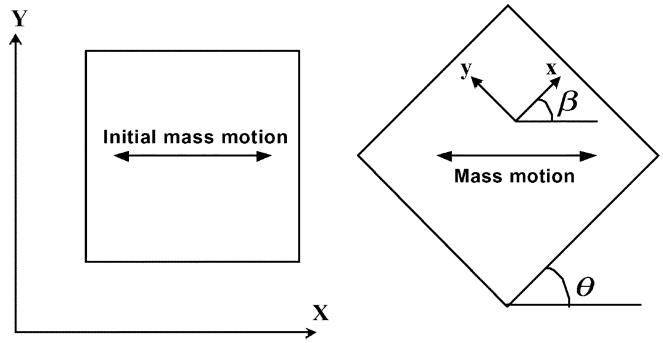

Fig. 2. Mass motion with initial X axis oscillation.

III. Angle Measurement

The proposed design for angle measurement is based on the principle of measuring the angle of free vibration of a suspended mass with respect to the casing of the gyroscope (Friedland and Hutton, 1978). A rough idea behind the methodology is as follows. If the mass is given an initial condition so that it vibrates in a known direction, the angle θ of the gyroscope in the global frame can be determined by keeping track of the angle, β, of the direction of vibration in the local frame (see Fig. 2). When the gyroscope experiences a rotation in the global frame, the mass rotates along with the gyroscope. However, as far as its vibration is concerned, it continues to vibrate in the same original direction with respect to the global frame. This result is stated formally and proved in Theorem 1.

Theorem 1: Consider the gyroscope system described by (1) and (2). Assume that the damping coefficients c_x and c_y are both zero and that the angular velocity $\dot{\theta}$ is constant. Assume that the initial conditions $y(0)$ and $\dot{y}(0)$ are both zero. Then the global response of the system for any nonzero initial conditions $x(0)$ and $\dot{x}(0)$ is vibration only along the global X axis.

Proof: The proof consists of first finding the local response of the system in coordinates $x(t)$ and $y(t)$ and then using transformation relations between local and global coordinates to find the global response $X(t)$ and $Y(t)$.

When $\ddot{\theta} = 0$, the equations in state–space form are

$$\frac{d}{dt}\begin{Bmatrix} x \\ \dot{x} \\ y \\ \dot{y} \end{Bmatrix} = \begin{bmatrix} 0 & 1 & 0 & 0 \\ \dot{\theta}^2 - \omega^2 & 0 & 0 & 2\dot{\theta} \\ 0 & 0 & 0 & 1 \\ 0 & -2\dot{\theta} & \dot{\theta}^2 - \omega^2 & 0 \end{bmatrix} \begin{Bmatrix} x \\ \dot{x} \\ y \\ \dot{y} \end{Bmatrix} \tag{3}$$

or

$$\dot{z} = Az.$$

The local state–space response of the system is therefore given by

$$z(t) = e^{At}z(0)$$

or

$$z(t) = L^{-1}\{(sI - A)^{-1}\}z(0) \tag{4}$$

where L^{-1} denotes the Laplace inverse.

$z(t)$ was evaluated using the Symbolic Toolbox in Matlab to calculate $L^{-1}\{(sI - A)^{-1}\}$ for the A matrix as given by (3). $x(t)$ and $y(t)$ are the first and third elements of the $z(t)$ vector.

For the case where $x(0) = 0$ and $\dot{x}(0) \neq 0, x(t)$ and $y(t)$ turn out to be

$$x(t) = \dot{x}(0)\frac{1}{2\omega}[\sin(\omega + \dot{\theta})t + \sin(\omega - \dot{\theta})t] \tag{5}$$

$$y(t) = \dot{x}(0)\frac{1}{2\omega}[-\cos(\omega - \dot{\theta})t + \cos(\omega + \dot{\theta})t]. \tag{6}$$

The global coordinates $X(t)$ and $Y(t)$ can be calculated from the transformation relations

$$X = x\cos(\theta) - y\sin(\theta) \tag{7}$$

$$Y = x\sin(\theta) + y\cos(\theta). \tag{8}$$

Substituting from (5) and (6) into (7) and (8), we have

$$Y(t) = \dot{x}(0)\frac{1}{2\omega}[\sin(\omega + \dot{\theta})t\sin(\theta) + \sin(\omega - \dot{\theta})t\sin(\theta) - \cos(\omega - \dot{\theta})t\cos(\theta) + \cos(\omega + \dot{\theta})t\cos(\theta)]$$

or

$$Y(t) = \frac{\dot{x}(0)}{2\omega}[-\cos\{(\omega - \dot{\theta})t + \theta\} + \cos\{(\omega + \dot{\theta})t - \theta\}]$$

or

$$Y(t) = \frac{\dot{x}(0)}{2\omega}[-\cos(\omega t) + \cos(\omega t)] = 0 \tag{9}$$

and

$$X(t) = \dot{x}(0)\frac{1}{2\omega}[\sin(\omega + \dot{\theta})t\cos(\theta) + \sin(\omega - \dot{\theta})t\cos(\theta) + \cos(\omega - \dot{\theta})t\sin(\theta) - \cos(\omega + \dot{\theta})t\sin(\theta)]$$

or

$$X(t) = \frac{\dot{x}(0)}{2\omega}[\sin(\omega t) + \sin(\omega t)]$$

or

$$X(t) = \frac{\dot{x}(0)}{\omega}\sin(\omega t). \tag{10}$$

Thus, the global response of the system is along the X axis, i.e., $Y(t) = 0$.

The proof follows along identical lines for the case where $x(0)$ is nonzero and $\dot{x}(0) = 0$. □

Remark: The result presented in Theorem 1 assumed that $\ddot{\theta} = 0$. However, the result also holds when the angular acceleration is nonzero, i.e., when the angular velocity is nonconstant. This result is difficult to prove analytically because the symbolic algebra is extremely complex when the analytical system is analyzed using the Matlab Symbolic Toolbox for $\ddot{\theta} \neq 0$. However, numerical simulations for a wide range of initial conditions $x(0)$ and $\dot{x}(0)$, incorporating $y(0) = 0, \dot{y}(0) = 0$, show that even when the angular acceleration is nonzero, the global vibration of the system is purely along the global X axis. Numerical simulation results are presented in Section IV.

IV. Energy Control

The method of measuring absolute angle presented in Section III relies on free vibration of the suspended mass. The presence of any damping will drive the free vibrations of the mass to zero. To overcome the affects of damping, energy needs to be added to the system. The energy can be added by using actuators to apply small forces to the x and y modes proportional to the x and y velocities, respectively. Such forces could counteract the damping in the system. If it were possible to select forces that would counteract the damping exactly (i.e., addition of negative damping), the mass would sustain free vibration indefinitely. However it is not possible to select such forces because of the changing damping of the system, manufacturing imperfections, temperature fluctuations and the presence of other energy loss mechanisms in the system. If the negative damping were chosen too large, the amplitude of motion will become unbounded, and if it were chosen too small, the amplitude of motion will still decay. In order to overcome this situation, a control loop is used to keep the total energy of the system constant. In this section, a feedback control system that adds energy and controls the energy of the system will be developed.

The current energy of the system is compared to the desired energy of the system and an energy error term is calculated. The forces counteracting the damping of the system are continuously adjusted using the energy error in order to keep the energy of the system constant:

$$F_x = \alpha\left(E - \frac{k_x}{2}x^2 - \frac{m}{2}\dot{x}^2 - \frac{k_y}{2}y^2 - \frac{m}{2}\dot{y}^2\right)\dot{x} \tag{11}$$

$$F_y = \alpha\left(E - \frac{k_x}{2}x^2 - \frac{m}{2}\dot{x}^2 - \frac{k_y}{2}y^2 - \frac{m}{2}\dot{y}^2\right)\dot{y} \tag{12}$$

where E is the energy set point, $((k_x/2)x^2 + (m/2)\dot{x}^2 + (k_y/2)y^2 + (m/2)\dot{y}^2)$ represents the instantaneous energy of the system and α is a feedback control gain that has units of s/m^2.

Theorem 2: The control system defined by (11) and (12) ensures that the steady-state energy of the closed-loop system is equal to

$$E - \frac{(\dot{x}^2 c_x + \dot{y}^2 c_y - mx\dot{x}\dot{\theta}^2 - my\dot{y}\dot{\theta}^2 + mx\dot{y}\ddot{\theta} - m\dot{x}y\ddot{\theta})}{\alpha(\dot{x}^2 + \dot{y}^2)}.$$

By increasing α, the steady-state energy of the system can be made approximately equal to the energy set-point E.

Proof: Equations (1) and (2) are modified to include the specific forces F_x and F_y applied by the control system

$$\ddot{x} = -\omega_x^2 x - \frac{c_x}{m}\dot{x} + x\dot{\theta}^2 + y\ddot{\theta} + 2\dot{\theta}\dot{y} + \frac{\alpha}{m}\left(E - \frac{k_x}{2}x^2 - \frac{m}{2}\dot{x}^2 - \frac{k_y}{2}y^2 - \frac{m}{2}\dot{y}^2\right)\dot{x} \tag{13}$$

$$\ddot{y} = -\omega_y^2 y - \frac{c_y}{m}\dot{y} + y\dot{\theta}^2 - x\ddot{\theta} - 2\dot{\theta}\dot{x} + \frac{\alpha}{m}\left(E - \frac{k_x}{2}x^2 - \frac{m}{2}\dot{x}^2 - \frac{k_y}{2}y^2 - \frac{m}{2}\dot{y}^2\right)\dot{y} \tag{14}$$

where α is a constant positive gain. Consider the following energy function for this system:

$$V = \frac{1}{2}m\dot{x}^2 + \frac{1}{2}m\dot{y}^2 + \frac{1}{2}kx^2 + \frac{1}{2}ky^2. \tag{15}$$

The time derivative of the energy function is

$$\dot{V} = m\dot{x}\ddot{x} + m\dot{y}\ddot{y} + kx\dot{x} + ky\dot{y} = \dot{x}[m\ddot{x} + kx] + \dot{y}[m\ddot{y} + ky]. \tag{16}$$

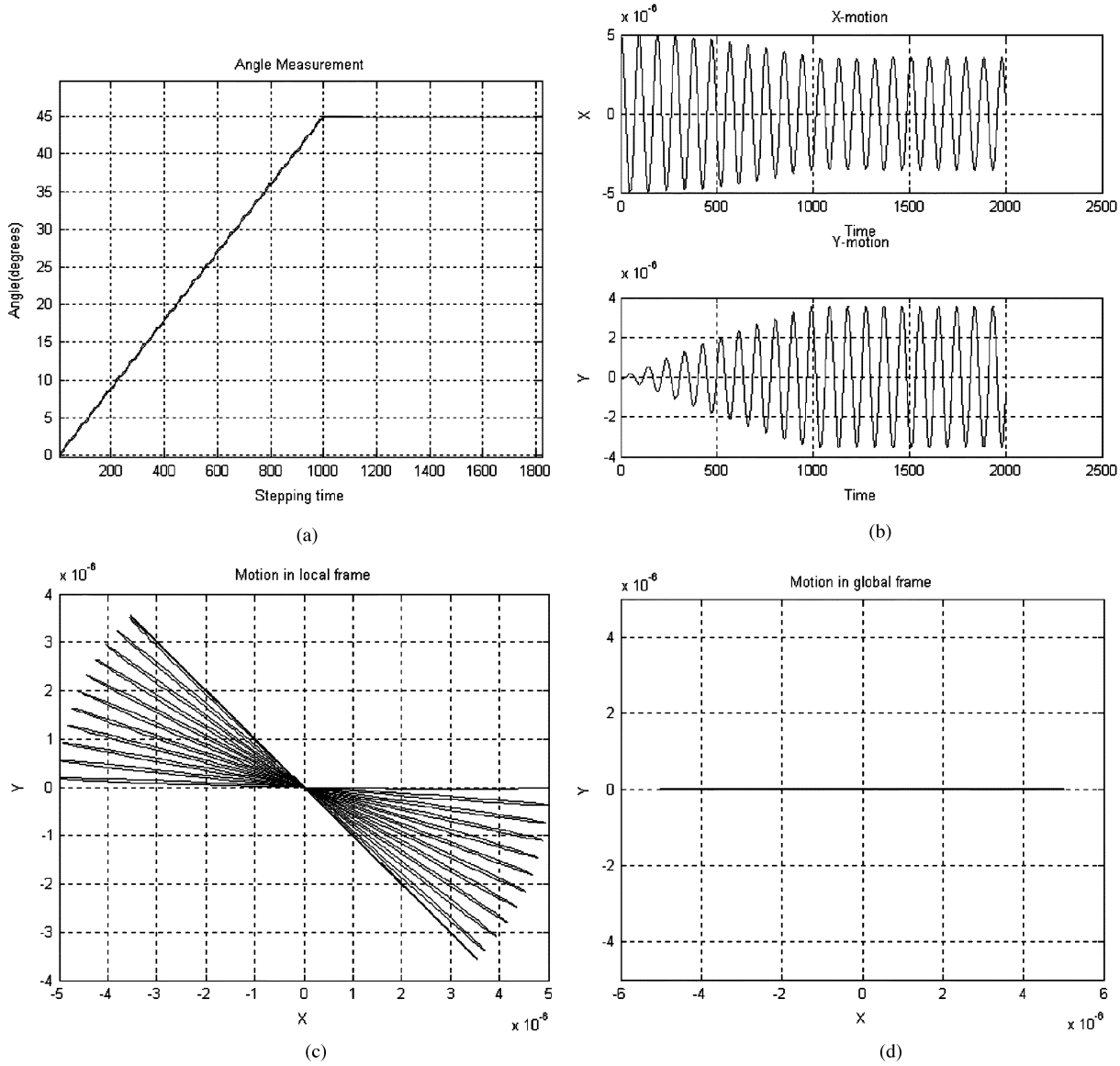

Fig. 3. Angle measurement. (a) Angular motion from 0° to 45°. (b) x and y motion. (c) Motion in gyroscope frame. (d) Motion in global frame.

Substituting (13) and (14) into (16) yields

$$\begin{aligned}\dot{V} = \dot{x}\Bigg[&-c_x\dot{x} + mx\dot{\theta}^2 + my\ddot{\theta} + 2m\dot{\theta}\dot{y} \\ &+\alpha\left(E - \frac{k}{2}x^2 - \frac{m}{2}\dot{x}^2 - \frac{k}{2}y^2 - \frac{m}{2}\dot{y}^2\right)\dot{x}\Bigg] \\ &+\dot{y}\Bigg[-c_y\dot{y} + my\dot{\theta}^2 - mx\ddot{\theta} - 2m\dot{\theta}\dot{x} \\ &+\alpha\left(E - \frac{k}{2}x^2 - \frac{m}{2}\dot{x}^2 - \frac{k}{2}y^2 - \frac{m}{2}\dot{y}^2\right)\dot{y}\Bigg] \qquad (17)\end{aligned}$$

or

$$\begin{aligned}\dot{V} = &\dot{x}^2[-c_x + \alpha(E - V)] + \dot{y}^2[-c_y + \alpha(E - V)] \\ &+ mx\dot{x}\dot{\theta}^2 + my\dot{y}\dot{\theta}^2 + my\dot{x}\ddot{\theta} - mx\dot{y}\ddot{\theta}. \qquad (18)\end{aligned}$$

This can further be rewritten as

$$\begin{aligned}\dot{V} + \alpha(\dot{x}^2 + \dot{y}^2)V = &-[\dot{x}^2c_x + \dot{y}^2c_y - mx\dot{x}\dot{\theta}^2 \\ &- my\dot{y}\dot{\theta}^2 + mx\dot{y}\ddot{\theta} - m\dot{x}y\ddot{\theta}] + \alpha(\dot{x}^2 + \dot{y}^2)E. \qquad (19)\end{aligned}$$

By inspection of (19), it is clear that the energy function V has stable dynamics. Thus, the energy of the x and y modes will always remain bounded implying that $x, y, \dot{x}, \dot{y}$ will also remain bounded. The steady-state of the energy function, V_{ss}, is

$$V_{ss} = E - \frac{(\dot{x}^2c_x + \dot{y}^2c_y - mx\dot{x}\dot{\theta}^2 - my\dot{y}\dot{\theta}^2 + mx\dot{y}\ddot{\theta} - m\dot{x}y\ddot{\theta})}{\alpha(\dot{x}^2 + \dot{y}^2)} \qquad (20)$$

By selecting an appropriate positive α, the steady-state of the energy function can be made close to the desired energy E. □

Numerical Simulations: Fig. 3 shows the simulated performance of the angle measurement gyroscope. In this simulation, the gyroscope frame experiences a ramp angular motion from 0° to 45° after which the angle remains at 45° as shown in Fig. 3(a). As seen in Fig. 3(c), the line of oscillation of the gyroscope moves from 0° to 45° in the local gyroscope frame. From the angle of this line of oscillation, the angular motion of the casing can be inferred. The line of oscillation in the global frame [as

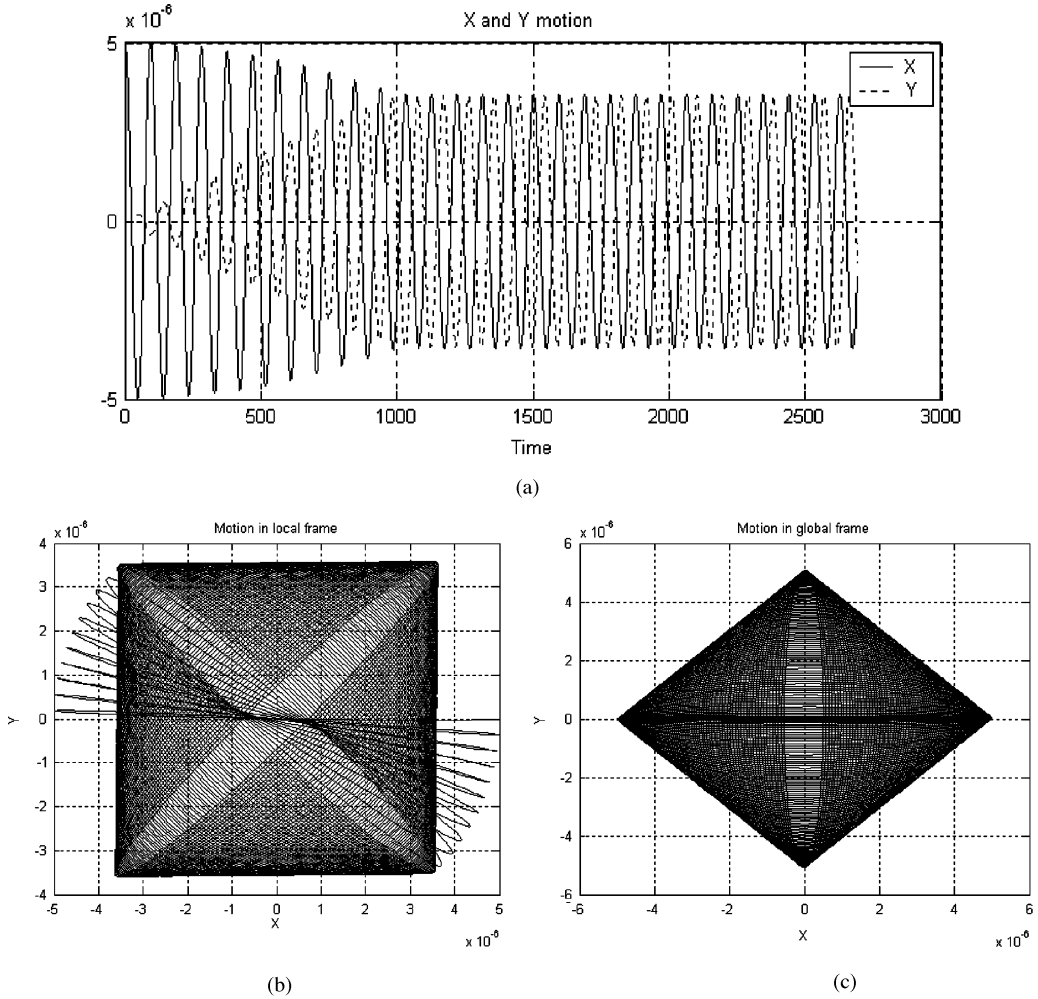

Fig. 4. Anisotropic oscillating. (a) x and y motion. (b) Motion in gyroscope frame. (c) Motion in global frame.

shown in Fig. 3(d)] always remains at 0°. The physical parameters used are typical values for MEMS gyroscopes [6]. The suspended mass is taken to be 0.9425e-6 kg. The spring stiffness for both x and y springs is 4180.8 and the damping coefficient is 0.2.

V. Angle Measurement in the Presence of Imperfections

A real MEMS gyroscope fabricated through many microfabrication steps will not be the ideal two-degrees of freedom (DOF) spring-mass system shown in Fig. 1. Common imperfections in fabrication are reflected as asymmetry in spring stiffness and damping. Also, cross-coupling forces occur along the two local axes when the mass orientation is not the same as that of the gyroscope frame. As shown in the following subsections, the presence of even small imperfections can have a huge impact on the performance of the above angle-measurement system. These imperfections must be handled before this theoretical sensing concept can be converted into a reliable practical sensor.

A. Mismatched Spring Stiffness Compensation

If the spring stiffness in the x and y axes are equal, the system is said to be isotropic. When the isotropic oscillator is allowed to freely oscillate, the precession of the straight line of oscillation provides a measure of the angle of rotation, as we have seen in the previous section. However, if the spring stiffness is not equal along the two axes, the mass no longer oscillates in a straight line even for a constant angle input. Instead, the line of oscillation keeps rotating around the frame. Fig. 4 shows the simulation results in both the local gyroscope frame and the global frame when there is a small 1% difference in the values of k_x and k_y. The angle input for the gyroscope casing is the same motion from 0° to 45° as discussed in the previous section.

In Fig. 4(b), the angle of vibration in the local axes keeps changing. This is also seen in Fig. 4(c), where the global axis of vibration keeps changing. Thus, even a small 1% difference between k_x and k_y causes the angle of free vibration to keep changing and never reach steady-state.

There will always be some difference between k_x and k_y due to manufacturing imperfections. One can attempt to compensate for the asymmetry actively using the F_x and F_y actuators. However, a direct compensation of the type

$$F_x = (-k_{\text{ref}} + k_x)x \tag{21}$$

$$F_y = (-k_{\text{ref}} + k_y)y \tag{22}$$

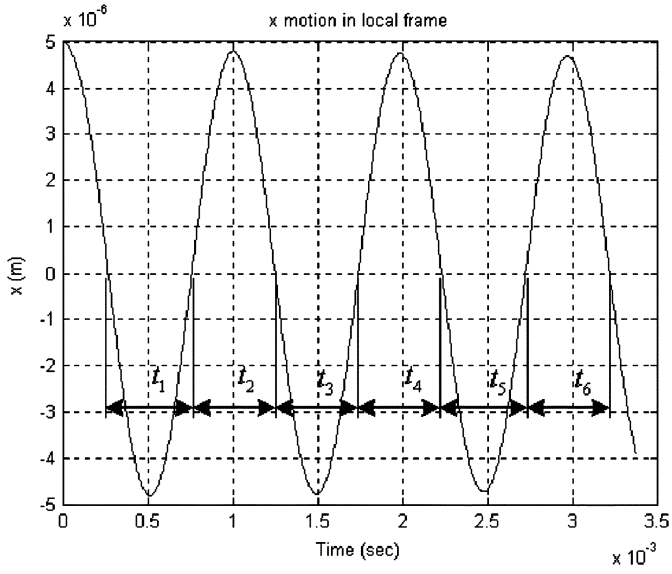

Fig. 5. Time interval measuring for stiffness value.

cannot solve the problem due to noise and bias in the measured values of k_x and k_y, as well as in the force generation of F_x and F_y.

The following control law is proposed instead:

$$\dot{F}_x = x[k_I(\hat{k}_x - \hat{k}_y) + k_p(\dot{\hat{k}}_x - \dot{\hat{k}}_y)] \quad (23)$$

$$\dot{F}_y = -y[k_I(\hat{k}_x - \hat{k}_y) + k_p(\dot{\hat{k}}_x - \dot{\hat{k}}_y)] \quad (24)$$

where $\hat{k}_x$ and $\hat{k}_y$ are measured stiffness values. The above forces tune both stiffness values to be equal to each other by integration of the difference between $\hat{k}_x$ and $\hat{k}_y$. $\hat{k}_x$ and $\hat{k}_y$ are measured stiffness values calculated from x and y measurement in real time as follows.

As shown in Fig. 5, the natural frequencies along each axes can be calculated by measuring the time interval of each half cycle

$$\omega_i = \frac{\pi}{t_i}, \quad i = 1, 2, 3, \ldots. \quad (25)$$

Then, the stiffness values can be calculated from the frequencies as

$$\hat{k}_i = m\omega_i^2 \quad (26)$$

where $\hat{k}$ is a periodic signal. Note that any errors in the assumed value of m will affect both $\hat{k}_x$ and $\hat{k}_y$ equally and will not result in a stiffness mismatch. Thus, this measuring scheme gives us a zero bias signal with the real stiffness value being equal to the mean value of the calculated signal

$$k_{\text{real}} = \frac{\sum_{i=1}^{N} \hat{k}_i}{N}. \quad (27)$$

Fig. 6 shows simulation results of using the above control law in the case where there is a 10% difference between k_x and k_y. It can be seen that the control law ensures that the mass vibrates along a steady-state straight line. The angle of rotation can be inferred from the angle of oscillation.

B. Addressing of Cross-Coupling Spring Stiffness

The springs along the two axes can develop cross-axes stiffness due to rotation of the suspended mass with respect to the gyroscope frame (Fig. 7). The ability of the springs to transmit forces perpendicular to their axis results in cross-coupling terms. The rotation of the mass with respect to the casing that can give rise to cross-axes stiffness can be modeled by the following equation [6]:

$$I\ddot{\phi} = -k_\phi \phi - I\ddot{\theta}. \quad (28)$$

Note that $I\ddot{\theta}$ represents the net effect of the external torques acting on the device. The angular motion between the mass and the casing is excited by the net external torque $I\ddot{\theta}$ and is resisted by the torsional stiffness k_ϕ.

The cross-axis stiffness is proportional to ϕ when ϕ is small because the component of the spring force that is perpendicular to the local axis is proportional to the angle ϕ. For the isotropic system with cross-axis stiffness, the overall equations of motion of the mass can be written as

$$\ddot{x} + 2\xi\omega\dot{x} + (\omega^2 - \dot{\theta}^2)x = -\frac{k_{yx}}{m}y + y\ddot{\theta} + 2\dot{\theta}\dot{y} \quad (29)$$

$$\ddot{y} + 2\xi\omega\dot{y} + (\omega^2 - \dot{\theta}^2)y = -\frac{k_{xy}}{m}x - x\ddot{\theta} - 2\dot{\theta}\dot{x} \quad (30)$$

where $k_{xy} = \gamma_{xy}\phi, k_{yx} = \gamma_{yx}\phi, \gamma_{xy} = k_{xx}, \gamma_{yx} = k_{yy}, k = \sqrt{(\omega_x^2 m)^2 - k_{xy}^2}$, and $\omega = \sqrt{k/m}$.

The cross-coupling forces result in ellipticity of the nominal straight-line motion and in frequency change, as can be seen in Fig. 8.

We can use the ability to simultaneously measure angular-rate and the observer of Section VI to estimate the measured angle accurately in the presence of the above imperfection. The observer (discussed in Section VII) ensures that the angle can be accurately estimated in spite of the elliptical motion.

C. Unequal Damping Compensation

Fig. 9 shows the performance of the system with unequal damping values in the x and y axes. The unequal damping values change the angle of rotation resulting in vibration along the axis with lower damping as shown in Fig. 9(a).

In order to overcome this problem, the energy control loop needs to be modified as follows. The damping terms c_x and c_y can be detected separately in the sensor calibration stage. The energy control forces from (3) and (4) should be modified to be

$$F_x = \alpha' \cdot c_x \cdot \left(E - \frac{\hat{k}_x}{2}x^2 - \frac{m}{2}\dot{x}^2 - \frac{\hat{k}_y}{2}y^2 - \frac{m}{2}\dot{y}^2 \right) \dot{x} \quad (31)$$

$$F_y = \alpha' \cdot c_y \cdot \left(E - \frac{\hat{k}_x}{2}x^2 - \frac{m}{2}\dot{x}^2 - \frac{\hat{k}_y}{2}y^2 - \frac{m}{2}\dot{y}^2 \right) \dot{y} \quad (32)$$

where the original equations have been modified using coefficients c_x and c_y. This modified control law compensates for the unequal damping by proportionately modifying the control gains for energy control along the two axes. Fig. 9(b) shows the effect of modified energy control at steady-state. We see that the steady-state error is gone but the vibrations of the mass now have an ellipticity instead of being a straight line. Again, to overcome

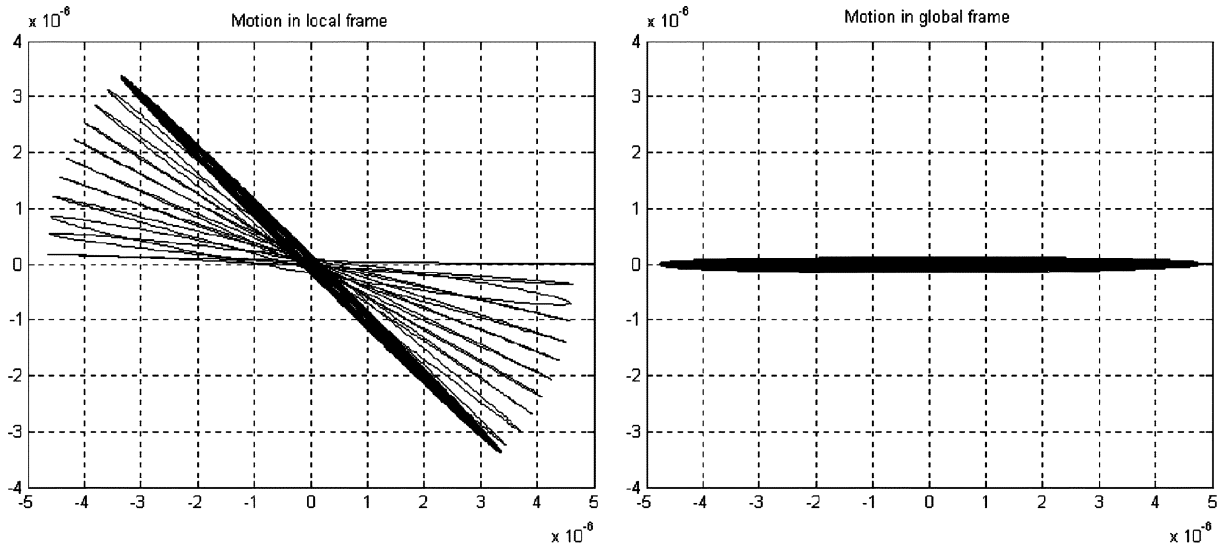

Fig. 6. Stiffness tuning control $\mathrm{ky} = 1.1 * \mathrm{kx}$. (a) Motion in gyroscope frame. (b) Motion in global frame.

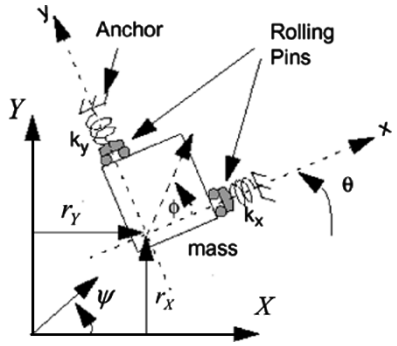

Fig. 7. Schematic representation of a simple mass spring system with two orthogonal modes [6].

the problem of ellipticity, we can use the observer (see Section VII) to get the estimated angle.

D. Addressing of Cross-Coupling Damping Effects

When the mass rotates an angle ϕ with respect to the local frame, the damping (quality factor) in both the x and y axes has cross-axis effects. In the symmetric stiffness system, the equations of motion can be written along the lines of (29) and (30) as

$$\ddot{x} + 2\zeta_{xx}\omega\dot{x} + (\omega^2 - \dot{\theta}^2)x = -2\zeta_{xy}\omega\dot{y} + y\ddot{\theta} + 2\dot{\theta}\dot{y} \quad (33)$$

$$\ddot{y} + 2\zeta_{yy}\omega\dot{y} + (\omega^2 - \dot{\theta}^2)y = -2\zeta_{xy}\omega\dot{x} - x\ddot{\theta} - 2\dot{\theta}\dot{x} \quad (34)$$

where $\zeta_{xy} = \gamma_d\phi, \zeta_{xx} = \sqrt{\zeta^2 - \zeta_{xy}^2}$ and $\zeta_{yy} = \sqrt{\zeta^2 - \zeta_{xy}^2}$ and γ_d is either $2\zeta_{xx}\omega$ or $2\zeta_{yy}\omega$.

The effect of cross-coupling damping is very small, as can be seen in Fig. 10 and use of the energy controller does not change the cross-coupling effect.

VI. Combined Angle and Angular-Rate Measurement

It is possible to combine the angular rate use of the gyroscope with its ability to measure angle. In this case,

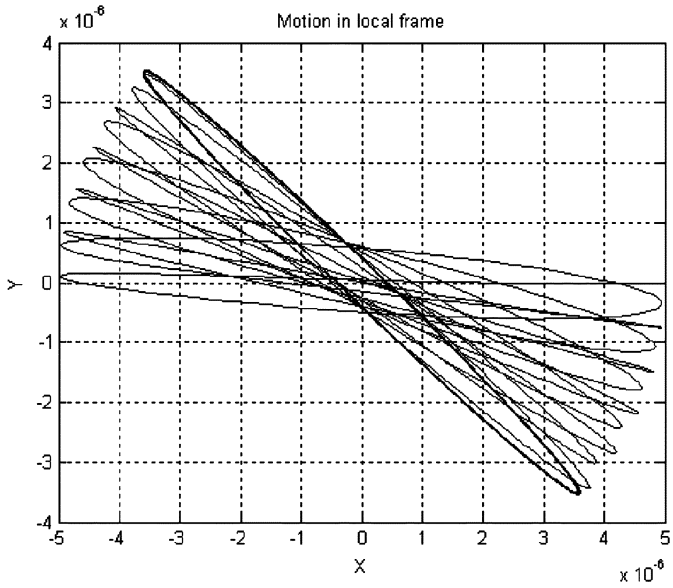

Fig. 8. Cross-coupling stiffness effect.

the x axis force is chosen to be a sum of the feedback force defined by (3) at steady-state and an additional sinusoidal excitation at a driven frequency ω_d

$$F_x = \alpha\left(E - \frac{\hat{k}_x}{2}x^2 - \frac{m}{2}\dot{x}^2 - \frac{\hat{k}_y}{2}y^2 - \frac{m}{2}\dot{y}^2\right)\dot{x} + F_d\sin(\omega_d t). \quad (35)$$

The y axis force remains the same as the energy control feedback force used for angle measurement

$$F_y = \alpha\left(E - \frac{\hat{k}_x}{2}x^2 - \frac{m}{2}\dot{x}^2 - \frac{\hat{k}_y}{2}y^2 - \frac{m}{2}\dot{y}^2\right)\dot{y}. \quad (36)$$

In the presence of an angular rate $\dot{\theta}$, the sinusoidal x axis excitation term in (35) causes vibrations along the y axis at the excitation frequency ω_d. The value of the angular rate can be

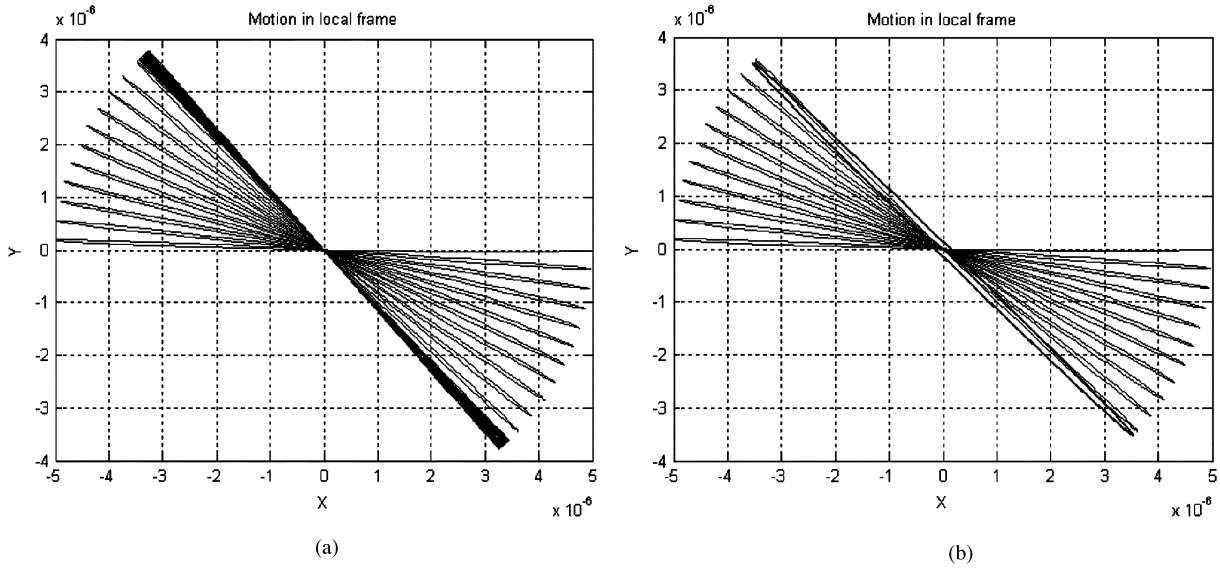

(a) (b)

Fig. 9. Asymmetric damping with energy control.

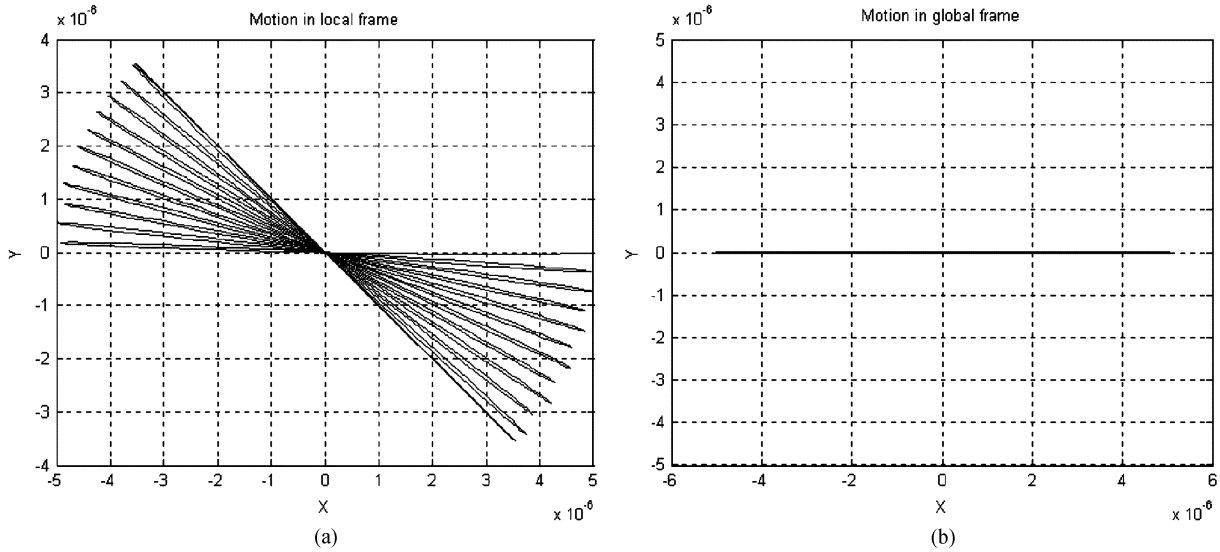

(a) (b)

Fig. 10. Cross-coupling oscillation for symmetric system with energy control. (a) Motion in local frame. (b) Motion in global frame.

obtained by demodulating the y axis motion at the driving frequency.

In implementing the above combined system, the x and y signals coming from the gyroscope need to go through a separate band pass filter at the natural frequency in order to determine the angle value. When running the gyroscope at both its natural frequency and the driving frequency the relative amplitude of oscillation at the two frequencies becomes important. It is necessary to ensure that the driving frequency ω_d is sufficiently far away from the natural frequency of the system. Roughly it was found that the free vibration signal provided a good measurement of the angular motion of the gyroscope as long as the driving frequency remained about an order of magnitude different from the natural frequency.

The results of running the gyroscope with both angular rate functionality and angle functionality are shown in Figs. 11 and 12 (the input signal was a sine wave with an amplitude of 1 rad and a frequency of 100 rad/s).

VII. Observer Estimation

If angle and angular rate are both measured by the gyroscope, an observer can be used to exploit the angular rate measurement so as to improve the absolute angle estimates. Consider the following observer:

$$\dot{\hat{\theta}} = \dot{\theta}_{\text{meas}} + K(\theta_{\text{meas}} - \hat{\theta}) \tag{37}$$

where θ_{meas} is the measured angle, $\dot{\theta}_{\text{meas}}$ is the measured angular rate, $\hat{\theta}$ is the estimate of the angle, $\dot{\hat{\theta}}$ is the estimate of the angular rate, and K is the observer gain. Using a small value for K will mean that the observer estimate is primarily obtained from integrating the angular rate with the angle measurement error serving mainly to correct the drift. A high value of K on the other hand will ensure that the observer relies more on the direct angle measurement with the angular rate measurement playing a role only for very high-frequency measurements.

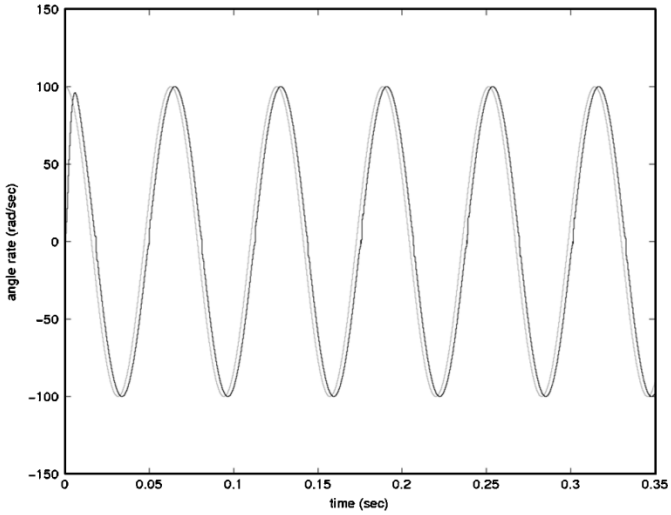

Fig. 11. Angular-rate signal.

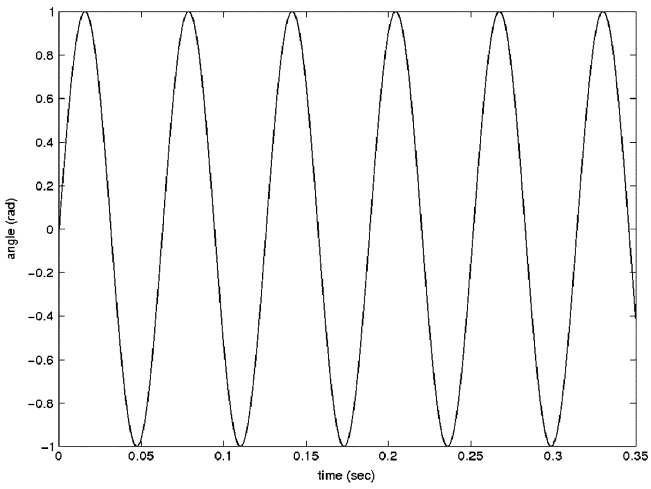

Fig. 12. Angle signal.

Based on the amount of ellipticity encountered in the angle measurement scheme and the drift present in the angular rate measurement scheme, the gain K can be chosen in an optimal way so as to obtain the best possible estimates of angular motion.

Angular estimates obtained using the observer are shown in Fig. 13.

VIII. MEMS Gyroscope Design

This section develops a MEMS design for the angle measurement device discussed in the previous sections. Electrostatic actuation is very popular in MEMS applications for its relatively high sensitivity and ease of fabrication [15], [16] and will be used for the proposed device. It is capable of generating large forces with high bandwidth. Comb drives used for electrostatic force actuation have two types of geometry. Lateral combs have a linear force displacement relationship but since their capacitance change relies on the area change they are less sensitive as sensors and produce less amount of electrostatic force as actuators. Transverse combs on the other hand are capable of producing higher forces as actuators and are more sensitive (i.e., capacitance change per displacement change is higher) if they are used as sensors despite they have a strictly nonlinear force-displacement relationship. The proposed absolute angle measurement gyroscopes have transverse (i.e., gap changing) comb drives for both actuation and sensing.

The proposed design is shown in Fig. 14. Two transverse comb actuators are used to provide forces in each direction (x and y) as well as for capacitive sensing. The resonant frequency range of the device is designed from about 150 to 300 Hz with a variety of mass and cantilever suspending beams design. The proposed gyroscope design has a central vibrating mass which is connected to the actuation and sensing comb structures by means of eight springs (i.e., four pairs of fixed-fixed end cantilever springs). The actuation and sensing comb drives are rigidly connected to the vibrating mass.

The voltage signals should be transferred from both sensing and actuation drives to the contact pads on the frame. Since the only connection from the comb drives is via the two springs on each side of the connecting centerpiece, these springs have to be used as the signal paths. However this necessitates electrical isolation, which is possible only if the two signal paths are physically separated from each other on the device layer. This problem of the necessity of electrical isolation and mechanical coupling was solved by designing free islands on the back-side of the device which hold the otherwise separated pieces on the device layer together.

The fabrication of the gyroscope will be based on deep reactive ion etch (DRIE) patterning on silicon on insulator (SOI) technology and is currently underway at the Nano Fabrication Center of the University of Minnesota. This high-yield process flow enables self-release of the high-aspect ratio devices eliminating the necessity of dicing after release.

Measurement Bandwidth: The nonlinear control system developed in this application can be implemented digitally using a microprocessor or an ASIC. The sampling frequency that can be achieved will limit the bandwidth of the angle measurement gyroscope. For instance, if a bandwidth of 1 kHz is required, then a sampling frequency of at least 10 kHz is desired. An alternate strategy to achieve a high bandwidth is to use a commercially available rate gyroscope and utilize the observer discussed in Section VII to combine rate measurement and angle measurement. Since the rate gyroscope can utilize analog electronics and can be a very high-bandwidth device, a high-bandwidth angle estimate can be obtained even if the bandwidth of the angle measurement sensor is itself low.

IX. Conclusion

MEMS gyroscope are typically designed to measure angular rate of rotation. A measurement of the angle itself is useful in many applications but cannot be obtained by integrating the angular rate due to the presence of bias errors which cause a drift. This paper presented an innovative design for a vibrating gyroscope that can directly measure both angle and angular rate. The design was based on the principle of measuring the angle of free vibration of a suspended mass with respect to the casing of the gyroscope. Several critical challenges had to be handled before the theoretical sensing concept can be converted into a

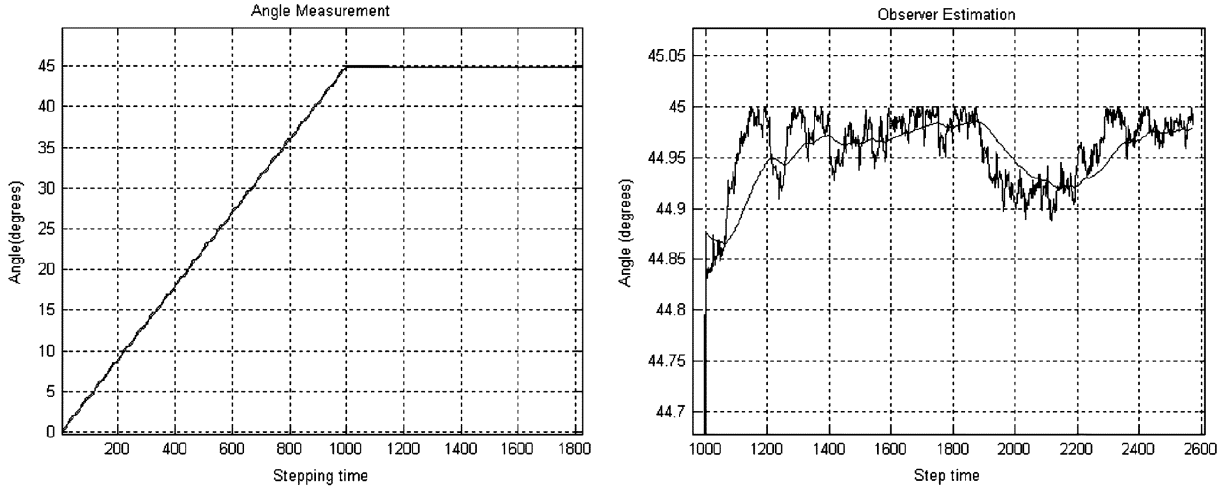

(a) (b)

Fig. 13. Observer estimation: raw measurement versus observer estimate.

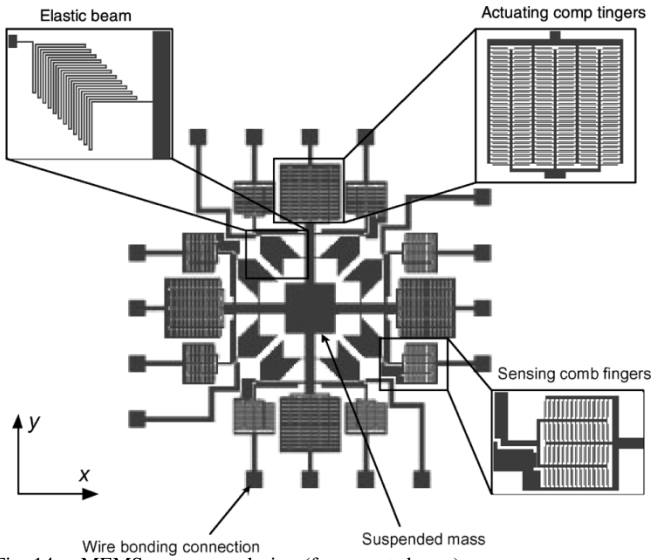

Fig. 14. MEMS gyroscope design (frame not shown).

reliable practical sensor. These included compensating for the presence of dissipative forces, mismatched springs, cross-axis stiffness and transmission of rotary torque. These challenges were addressed by the development of a composite nonlinear feedback control system that compensated for each of the above effects and ensured that the mass continued to behave as a freely vibrating structure. Theoretical analysis and simulation results presented in the paper showed that the gyroscope can accurately measure both angle and angular rate for low-bandwidth applications.

REFERENCES

[1] J. Bernstein *et al.*, "A micro-machined comb-drive tuning fork rate gyroscope," in *Proc. Workshop Microelectromechanical Systems*, 1993, pp. 143–148.

[2] W. A. Clark *et al.*, "Micro-machined *Z*-axis vibratory rate gyroscope," in *Proc. Tech. Dig. Solid State Sensors and Actuators Workshop*, 1996, pp. 283–287.

[3] D. S. Eddy and D. R. Sparks, "Application of MEMS technology in automotive sensors and actuators," *Proc. IEEE*, vol. 86, no. 8, pp. 1747–1755, Aug. 1998.

[4] J. W. Gardner, *Microsensors: Principles and Applications*. New York: Wiley, 1994.

[5] T. Juneau *et al.*, "Dual axis operation of a micromachined rate gyroscope," in *Proc. Tranducers'97*, vol. 2, 1997, pp. 883–886.

[6] M. Kranz and G. K. Fedder, "Design, simulation, and implementation of two novel micromechanical vibratory-rate gyroscopes," Dept. Elect. Comput. Eng., Carnegie-Mellon Univ., Philadelphia, PA, May 1998.

[7] A. Lawrence, *Modern Inertial Technology*. New York: Springer-Verlag, 1998.

[8] Y. Mochida, M. Tamura, and K. Ohwada, "A micromachined vibrating rate gyroscope with independent beams for the drive and detection modes," *Sens. Actuators A, Phys.*, vol. 80, pp. 170–178, 2000.

[9] A. M. Shkel, R. Horowitz, A. A. Seshia, S. Park, and R. T. Howe, "Dynamics and control of micromachined gyroscopes," in *Proc. Amer. Control Conf.*, vol. 3, 1999, pp. 2119–2124.

[10] M. Putty and K. Najafi, "A micro-machined vibrating ring gyroscope," in *Proc. Tech. Dig. Solid-State Sensors and Actuators Workshop*, Jun. 13–16, 1994, pp. 213–220.

[11] R. Rajamani, H. S. Tan, B. Law, and W. B. Zhang, "Demonstration of integrated lateral and longitudinal control for the operation of automated vehicles in platoons," *IEEE Trans. Contr. Syst. Technol.*, vol. 8, no. 4, pp. 695–708, Jul. 2000.

[12] J. J. Slotine and W. Li, *Applied Nonlinear Control*. Englewood Cliffs, NJ: Prentice-Hall, 1991.

[13] E. H. Tseng, B. Ashrafi, D. Madau, T. A. Brown, and D. Recker, "The development of vehicle stability control at ford," *IEEE/ASME Trans. Mechatronics*, vol. 4, no. 3, pp. 223–234, Sep. 1999.

[14] MCNC MEMS Technology Applications Center, Research Traingle Park, NC, Oct. 1994. rev. 3.

[15] W. C. Tang, M. G. Lim, and R. T. Howe, "Electrostatic comb drive levitation and control method," *J. Microelectromech. Syst.*, vol. 1, no. 4, pp. 170–178, Dec. 1992.

[16] T. Harness and R. R. A. Syms, "Characteristic modes of electrostatic comb-drive *X–Y* microactuators," *J. Miromech. Microeng.*, vol. 9, pp. 1–8, 1999.

[17] B. Friedland and M. Hutton, "Theory and error analysis of vibrating-member gyroscopes," *IEEE Trans. Autom. Control*, vol. AC–23, no. 4, pp. 545–556, Aug. 1978.

Damrongrit Piyabongkarn received the B.Eng. degree in mechanical engineering from Chulalongkorn University, Bangkok, Thailand, in 1996 and the M.S. degree in mechanical engineering from the University of Texas, Arlington, in 2000. He is currently working toward the Ph.D. degree in mechanical engineering at the University of Minnesota, Minneapolis.

His research interests include advanced controls, MEMS sensor design, signal processing, and vehicle dynamics and control.

Mr. Piyabongkarn received the 2003–2004 Doctoral Dissertation Fellowship from the University of Minnesota.

Rajesh Rajamani received the M.S. and Ph.D. degrees from the University of California at Berkeley in 1991 and 1993, respectively, and the B.Tech. degree from the Indian Institute of Technology, Madras, India, in 1989.

He spent five years working as a Research Engineer at United Technologies Research Center (UTRC) and then at California PATH. He is currently an Associate Professor in the Department of Mechanical Engineering, University of Minnesota, Minneapolis. His active research interests include intelligent transportation systems, MEMS sensor design, active noise control, fault diagnostics, and control design and state estimation for nonlinear systems. He has authored over 60 refereed publications and received two patents.

Dr. Rajamani has won several awards including the CAREER Award from the National Science Foundation, the 2001 Outstanding Paper Award from the IEEE TRANSACTIONS ON CONTROL SYSTEMS TECHNOLOGY, the Distinguished Service Team Award from the University of California at Berkeley, and the Outstanding Achievement of the Year Award from United Technologies Research Center.

Michael Greminger received the B.S. and M.S. degrees in mechanical engineering from the University of Minnesota, Minneapolis, in 2000 and 2002, respectively, and is currently working toward the Ph.D. degree in mechanical engineering at the University of Minnesota.

His research interests include microrobotics, microassembly, and computer vision.

Mr. Greminger received the Computational Science Graduate Fellowship (CSGF) from the Department of Energy.